The Potential of LEO-PNT Mega-Constellations for Ionospheric 3-D Imaging: A Simulation Study

Fabricio S. Prol, Artem Smirnov, Sanna Kaasalainen, Mohammad Mainul Hoque, Mohammad Zahidul H. Bhuiyan, and Francesco Menzione

***Abstract*—The rapid increase of the number of low Earth orbit (LEO) satellites brings up the possibility of LEO satellite missions transmitting dedicated signals for positioning, navigation, and timing (PNT). Although great attention has been paid in recent years to understand the benefits of LEO satellites for PNT, dense LEO constellations will also provide unique measurements of the Earth's upper atmosphere. The benefits of the highly dense LEO-PNT systems are explored in this work to analyze the potential gains of using total electron content (TEC) measurements derived from LEO-PNT systems for 3-D ionospheric imaging. As a result, we have found obvious improvement in the ionospheric imaging system by including LEO satellites to the system geometry. Furthermore, our investigation has discovered that accurate electron density representations can be obtained even when no horizontal viewing angles are included in the imaging system, which is a unique point to imaging systems. In addition, we propose a method to derive accurate 3-D electron density representation based on ranging measurements from intersatellite links. The method provides accurate electron density estimations with no evident bias, but it still depends on the accuracy of background representations. The results indicate that improvements of over 80% can be achieved for both vertical and horizontal distributions of the ionosphere in comparison to the background.**

***Index Terms*—Global navigation satellite systems (GNSS), ionospheric imaging, ionospheric tomography, low Earth orbit (LEO)-positioning, navigation, and timing (PNT), simulated dataset.**

I. Introduction

OVER the next decade, thousands of satellites placed in low Earth orbit (LEO) will be available. The decline in costs of building and maintaining LEO satellites has brought up a possibility to develop highly dense satellite constellations, named mega-constellations. Several simulations have been performed in the recent years to understand the potential of these future LEO mega-constellations for applications ranging from broadband communication [1], [2], [3] to satellite-based positioning [4], [5], [6], [7], [8], [9]. The most recent simulations [10], [11] have shown that LEO satellites can bring considerable gains to positioning, navigation, and timing (PNT) in comparison to classic global navigation satellite systems (GNSS), since stronger signals and better geometry can be offered to users on the ground. Given these benefits, aspirations to build LEO-positioning, navigation, and timing (PNT) systems do exist. Large investments to develop LEO-PNT systems have already been made by Xona Space System [12], in the USA; the European Space Agency (ESA) [13], in Europe; the Jiuquan Satellite Launch Center [14], in China; and the indoor navigation from CubeSat technology (INCUBATE) project [15], in Finland. Moreover, the fused architecture [16] as well as the possibility to embark hosted navigation payloads [17] has the potential to extend the LEO-PNT paradigm to all preexistent or upcoming mega-constellations. In this direction, the Starlink mega-constellation contains more than 4000 satellites and enables carrier phase measurements to be extracted [18].

Although many studies have focused on improving PNT solutions, the upcoming LEO-PNT systems can be alternatively used to extract ionospheric parameters [19]. This can be accomplished even when only single-frequency data are accessible [20], depending on the frequency utilized by the system. Like in classic GNSS [21], dedicated LEO-PNT systems will likely provide carrier-phase and pseudorange measurements to users on the ground, which can be rather used to compute the total electron content (TEC) and generate valuable representations of the ionosphere in 2-D. A major drawback in the ionospheric imaging based on GNSS, however, is the incomplete geometrical coverage of the GNSS ray paths to estimate the vertical distribution of the ionosphere in 3-D representations [22], [23]. Despite the progress in the development of ionospheric tomography [24], [25], [26], [27], data ingestion [28], and data assimilation [29], [30], 3-D ionospheric imaging is currently an ill-conditioned and ill-posed inverse problem due to the GNSS poor geometry [31]. With the expected better geometry coverage by LEO satellites, upcoming LEO-PNT systems can likely provide gains in the 3-D ionospheric imaging.

Another possible benefit of dedicated LEO-PNT systems to 3-D ionospheric imaging is regarded to the intersatellite links

Manuscript received 25 May 2023; revised 6 July 2023; accepted 14 July 2023. Date of publication 27 July 2023; date of current version 22 August 2023. This work was supported in part by the INdoor navigation from CUBesAT Technology (INCUBATE) project, under Grant from the Technology Industries of Finland Centennial Foundation and in part by the Jane and Aatos Erkko Foundation. *(Corresponding author: Fabricio S. Prol.)*

Fabricio S. Prol, Sanna Kaasalainen, and Mohammad Zahidul H. Bhuiyan are with the Department of Navigation and Positioning, Finnish Geospatial Research Institute, National Land Survey of Finland, 02150 Espoo, Finland (e-mail: fabricio.dossantosprol@nls.fi; sanna.kaasalainen@nls.fi; zahidul.bhuiyan@nls.fi).

Artem Smirnov is with the Helmholtz Centre Potsdam, GFZ German Research Centre for Geosciences, 14473 Potsdam, Germany, and also with the Institute of Physics and Astronomy, University of Potsdam, 14469 Potsdam, Germany (e-mail: asmirnov@gfz-potsdam.de).

Mohammad Mainul Hoque is with the German Aerospace Center, Institute for Solar-Terrestrial Physics, 17235 Neustrelitz, Germany (e-mail: mainul.hoque@dlr.de).

Francesco Menzione is with the European Commission-Joint Research Centre, 21027 Ispra, Italy (e-mail: francesco.menzione@ec.europa.eu).

Digital Object Identifier 10.1109/JSTARS.2023.3299415

(ISL). The ISL data in satellite-based navigation systems were initially proposed to reduce the GNSS dependence on the ground segment and help the implementation of an autonomous navigation [32]. Later, several studies have demonstrated that ISL can be effectively used to improve the orbit determination due to the intersatellite range measurements [33], [34], [35], [36]. Nevertheless, these studies considered GNSS satellites located at medium Earth orbit (MEO). In case of LEO satellites, as they are immersed in the ionosphere, there is an opportunity to estimate the ionospheric delay in the ray path between the satellites [37] and improve the overall 3-D ionospheric imaging.

The need for improved and global-scale electron density models has been widely acknowledged and enhanced along with the increasing space activity. Numerous studies, including those utilizing GNSS, have been carried out during the decades (see, e.g., [25], [38], [39], [40]). To investigate the potential gains that dense LEO-PNT systems can bring to the understanding of the ionospheric dynamics, this study explores how LEO satellites can improve the 3-D ionospheric imaging. We do not seek to analyze any seasonal behavior of the ionosphere, any phenomena at a specific region and period, or any real scenario of a GNSS network. The intention is to analyze the possible benefits of using LEO satellite to improve ionospheric background models by TEC data inversion techniques assuming great satellite coverage. The investigation covers distinct types of measurements that dedicated LEO-PNT systems can provide, including ground-based observations (from LEO to the ground and GNSS to ground), TEC observations retrieved by GNSS receivers onboard LEO satellites, and ISL measurements between LEO satellites.

The rest of this article is organized as follows. In Section III, a simulated dataset is presented to evaluate the geometry benefits of placing LEO satellites at several orbital altitudes. The results are presented in Section IV. Finally, Section V concludes this article.

II. Method

This section presents the two methods used to analyze the benefits from LEO satellites. First, Section II-A shows the 3-D imaging method developed to invert ground- and satellite-based TEC measurements into electron densities. Next, in Section II-B, we show a method specifically developed in this work to use the intersatellite links.

A. TEC Data Inversion With Ground-Based and POD Observations

The basic quantity to represent the ionosphere and plasmasphere in inversion algorithms is the TEC, i.e., the integral of the electron density N_e along the path length (l) between a satellite s and the receiving antenna r. The TEC is counted in a column whose cross-sectional area is equivalent to 1 m^2 and expressed as

$$\text{TEC} = \int_r^s N_e dl \tag{1}$$

being usually represented as TEC units (TECU), where 1 TECU $= 10^{16}$ el/m^2.

To build an equation system and parameterize the electron density unknowns based on TEC measurements, the ionosphere and plasmasphere are typically broken down into a grid of voxels. The TEC in (1) is then approximated by the following finite sum:

$$\text{TEC} = \sum_{j=1}^{J} N_{e_j} d_{ij} \tag{2}$$

where N_{e_j} is the electron density corresponding to the voxel j and d_{ij} is the path length of the signal i inside the voxel j. The finite sum is performed ranging from 1 to J (number of voxels in the grid) and d_{ij} is zero at voxels not intersected by signal i.

Based on (2), the following equation system is built:

$$\mathbf{y} = \mathbf{A}\mathbf{x} + \epsilon \tag{3}$$

where $\mathbf{y}$ is a vector of TEC measurements, $\mathbf{x}$ is the unknown vector of electron densities, $\mathbf{A}$ is the Jacobian matrix of the system, composed by the path lengths d_{ij}, and ϵ is a vector of measurement noises and discretization errors.

The unknown $\mathbf{x}$ can be solved by several algorithms, such as least squares, Kalman filters, best linear unbiased estimators, singular value decomposition, and variational methods. One of the first implementations to solve the TEC inversion problem was applied by [41]. They applied a well-known tomography method named algebraic reconstruction technique (ART), which solves the problem by incorporating purely geometrical relations. In case the system geometry is strong (i.e., it is a well-posed system), the solution converges to the expected results. However, as the poor GNSS geometry makes the system ill-posed, the solution is usually not straightforward. Typically, a background (i.e., an initial guess) is required to help the estimator, and a regularization process is often included to smoothly cover the voxels not crossed by any TEC measurements [42].

As the main interest of this work is to evaluate how LEO satellites can improve the system geometry, the purely geometric ART algorithm is selected to perform the TEC data inversion. The ART algorithm is implemented with the following iteration process [43]:

$$N_{e_j}^{k+1} = N_{e_j}^{k} + w \frac{\text{TEC}_i - \sum_{j=1}^{J} d_{ij} N_{e_j}^{k}}{\sum_{j=1}^{J} d_{ij}^2} d_{ij} \tag{4}$$

where $N_{e_j}^{k+1}$ is the estimated electron density in iteration $k+1$ and w is a weighting parameter, empirically selected as $w = 0.2$.

Most ART applications are based on ground GNSS stations. The ray paths between ground and GNSS satellites flying at around 20 000 km cross the entire ionosphere, allowing to recover ionospheric distributions. Due to the poor GNSS geometry, TEC measurements obtained by GNSS receivers onboard LEO satellites for precise orbit determination (POD) are often included to help the estimator [44], [45]. However, as shown in the results section of the current work, merging ground- and POD-based measurements are still not enough to accurately map the ionosphere. To further improve the estimation, we also include TEC measurements obtained by dense LEO-PNT systems. Fig. 1 shows a schematic of the ray path geometries used to merge the observations from GNSS and LEO satellites.

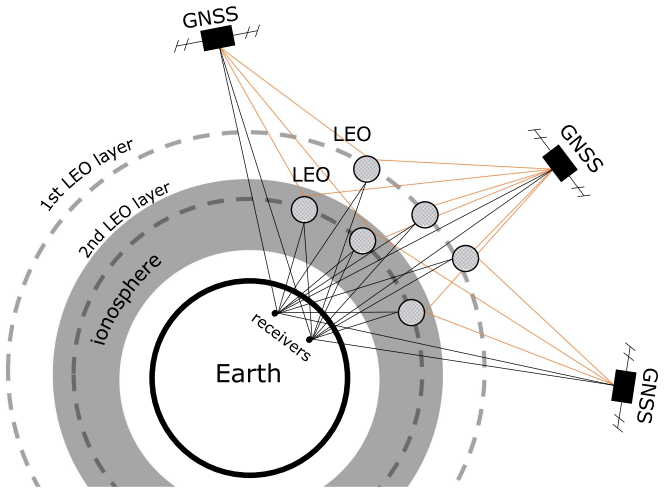

Fig. 1. Ray path geometries provided by GNSS satellites and dedicated LEO satellites to PNT. Ground-based receivers are supposed to receive and process both GNSS and LEO-PNT signals. GNSS receivers onboard the LEO satellites complete the system geometry.

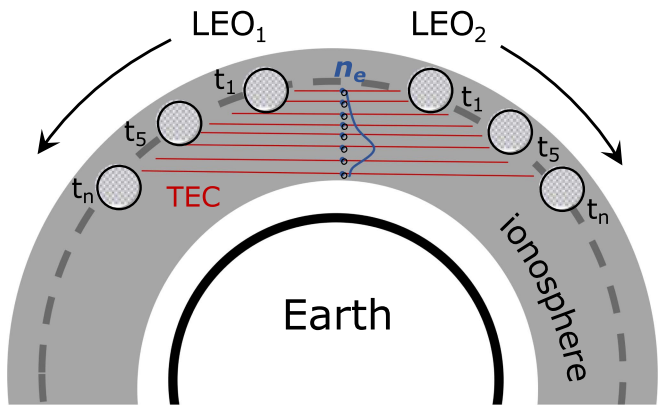

Fig. 2. Ray path geometry by the ISL measurements observed between two LEO satellites (LEO_1 and LEO_2). This conceptual example shows the TEC measurements taken at t_n time instances while the LEO satellites are progressing in opposite directions over time. The averaged electron density is retrieved at the central point of the ray paths, forming an ionospheric profile.

The primary types of observations to solve (4) are obtained by ground GNSS stations, POD receivers onboard LEO satellites, and ground stations receiving GNSS-like signals transmitted by LEO satellites. No LEO satellite system can currently provide the latter type of observation; however, we plan to evaluate the benefits of including them into the estimation process.

B. TEC Data Inversion With ISL Measurements

The ISL data in satellite-based PNT systems consist of ranging measurements between the satellites [34], [46]. They improve the orbit determination and synchronize the satellites to the same time standards. As LEO satellites are immersed in the ionosphere, there is an opportunity to estimate the ionospheric delay and the consequent TEC values in the ray path connecting them. The measurements can be directly used to solve (3). However, they will most likely cover just a small portion of the ionosphere and vaguely help the estimator. To better exploit these measurements, we propose a different form to carry out the TEC inversion, considering the unique geometry provided by the LEO-based ISL data.

Fig. 2 shows a schematic of the geometry obtained with the ISL measurements. The distribution of ISL measurements can be complicated by the effective network topology, i.e., intra- and interplane connections availability. In this example, two LEO satellites in the same orbital plane are flying in opposite directions. The TEC measurements, assumed to be taken as straight lines, are tracked in distinct times $(t_1, t_2, \ldots, t_n)$. As the satellites move apart, the TEC values cover a large path length, but the ray path keeps crossing a central point in which the electron density N_e is retrieved. The central point is coincident with the closest point to the Earth in the ray path and is also known as the tangent point (TP) in radio occultation (RO) techniques [47], [48]. In principle, the onion peeling approach [49], commonly used in GNSS RO techniques, can be used to estimate the electron density. However, the geometry shown in Fig. 2 slightly differs from those obtained in GNSS RO techniques. Since the transmitter is also located in LEO orbits, a much faster TEC variability is experienced. Hence, the issues with the spherical symmetry assumption [50], [51], [52], typically employed when using GNSS RO techniques, are enlarged.

Another approach to invert the TEC measurements into electron densities is inspired by the studies conducted with the gravity recovery and climate experiment (GRACE) satellites. The GRACE satellites comprise two LEO spacecraft, GRACE-A and GRACE-B, which follow each other at a distance of about 200 km. The TEC between the two spacecraft is deduced from the ranging measurements of the K-band ranging (KBR) system. As shown by [53], the averaged electron density can be obtained by dividing the horizontal TEC by the distance between the spacecraft. This technique has proven to provide a highly accurate electron density measure, in excellent agreement with incoherent scatter radar (ISR) observations [54]. Given the requirement that the LEO satellites are close enough, the same principle can be applied to the ISL data between LEO satellites. Indeed, highly dense LEO constellations will likely meet this basic requirement of short distances at certain time instances.

To investigate how the method adopted by the GRACE KBR ranging system would perform in case of LEO satellites, we evaluate the electron density accuracy obtained by dividing the horizontal TEC by the distance between LEO satellites. At the time instance t_n, given that the LEO satellites are close enough ($<$200 km), the electron density is retrieved by

$$N_e^{t_n} = \frac{\mathrm{TEC}^{t_n}}{R^{t_n}}. \tag{5}$$

R being the distance between the LEO satellites obtained by the satellites POD.

Notice that (5) does not include the bias associated with the noncalibrated TEC measurements. In the GRACE KBR system, the bias is retrieved based on external data source obtained by CHAMP and ISR electron density measurements. In the current study, the external data source is similarly considered available. Then, we can investigate the direct performance of the retrieved electron density with (5).

Equation (5) provides an accurate estimation in case the electron density represents the average electron density in the

whole path between the two LEO satellites (LEO_1 and LEO_2). This condition seems to hold for the GRACE satellites; however, as the LEO satellite moves apart, the averaged electron density in between the satellites is affected by the nonspherical symmetry of the ionosphere. This means that the TEC between the TP and LEO_1 is considerably different from the TP and LEO_2 in larger distances due to the horizontal gradients of the ionosphere. To account for this effect, the developed method utilizes background information of the ionosphere. The background is used to correct the nonspherical symmetry by the following equation:

$$N_e^{t_n} = \frac{\mathrm{TEC}^{t_n}}{R^{t_n}} N_{e_0}^{t_n} \left(\frac{\mathrm{TEC}_0^{t_n}}{R^{t_n}} \right)^{-1} \tag{6}$$

where N_{e_0} and TEC_0 stand for the electron density and TEC values computed with the background, respectively. Indeed, the right-side term of (6) acts as a correction factor to the nonspherical symmetry of the ionosphere. The retrieved accuracy will therefore heavily depend on the ability of the background to represent the horizontal gradients of the ionosphere.

III. Simulated Dataset

As a basis for the analysis, a simulated dataset was created to generate TEC measurements for the data inversion and quality evaluation. Section III-A shows how the ionosphere and plasmasphere electron densities are simulated. Then, Section III-B shows how the receiver and transmitters are virtually generated to compute the virtual TEC measurements.

A. Simulated Ionosphere and Plasmasphere

To simulate the ionosphere and plasmasphere, a global 3-D grid is constructed with a horizontal resolution of 2° in latitude by longitude, and vertical resolution of 10 km in altitude, ranging from 50 to 20 000 km. Each voxel is then filled with a simulated electron density. The simulation is computed to represent two cases: 1) the background and 2) the "real" electron density field. The background is usually obtained from empirical models of the ionosphere (see the following references) to provide an initial guess of the electron density. The "real" electron density fields, referred to as the reference dataset, are used to represent the expected ionosphere/plasmasphere, i.e., the ideal values to be obtained by the TEC inversion technique.

1) *Background Ionosphere/Plasmasphere*: The background is created with the Neustrelitz electron density model (NEDM) [55]. This model is established by superposing the E- and F-layers in the ionosphere with two exponential decay functions in the plasmasphere. The driving parameter of the electron density is the solar radio flux index F10.7. A comprehensive validation study was conducted by [55], showing that the NEDM represents the climatological patterns of the ionosphere and plasmasphere in comparison to several ground- and satellite-based observations acquired with GNSS, in-situ, and RO instruments.
2) *Reference Ionosphere/Plasmasphere*: The electron density distribution assumed as reference to this work is created by merging a set of state-of-the-art models of the ionosphere and plasmasphere. The bottomside ionosphere is represented by IRI-2016 [56] supported by external values of the F2-peak density (NmF2) and height (hmF2). The external NmF2 and hmF2 values are obtained by the neural network-based model of electron density in the topside ionosphere (NET) [57]. The topside ionosphere (up to 1000 km) is also computed by the NET model since it outperforms the IRI-2016 model in the ionospheric peak height and above. Above 1000 km, the electron density is retrieved with the model developed by [58], which is suitable to concatenate the topside ionosphere with the plasmasphere. The driving parameters of the combined model are the solar radio flux index P10.7 [59], the planetary Kp index, and the symmetric ring current SYM-H index, which shows the strength of the geomagnetic storms. This unified model provides good estimations not only in the profile shapes but also in the TEC magnitude and distributions. Nevertheless, to improve the TEC accuracy even further, we rescale the NmF2 values obtained by NET to match the vertical TEC (VTEC) values provided by the international GNSS service (IGS), under the form of global ionospheric maps (GIMs). The GIM produced by the Center for Orbit Determination in Europe (CODE) is selected since it is one of the best behaving IGS GIMs [60].

The background and reference models are applied on November 06, 2022, 00:00 h UT (universal time). This day is selected since no evident storms have occurred in the period and because there are several GNSS satellites in operational phase, including GPS, GLONASS, Galileo, and Beidou systems. The driving parameters are defined as P10.7 = 130.373 sfu (solar flux units), Kp = 0.7, and SYM-H = −17 nT. Fig. 3 shows the obtained VTEC maps with the simulated electron density distributions used as a reference (top panels) and as background (bottom panels). Four example cases are shown. The first one refers to the VTEC values computed from 800–20 000 km with the simulated dataset. The second example refers to the VTEC values from 500–20 000 km. These two examples simulate VTEC maps observed by GNSS receivers onboard LEO satellites for POD. The third example shows VTEC values computed from 50–500 km. This simulates the VTEC maps that can be obtained in case the LEO satellite is deployed at 500 km, as dedicated systems for PNT, i.e., a user on the ground is capable of tracking GNSS-like signals from a satellite flying at 500 km. The last example simulates a VTEC map typically observed by GNSS systems, i.e., ranging from the ground up to 20 000 km.

To better visualize the simulated dataset, Fig. 4 shows four scenarios of electron density distributions in terms of longitude by the altitude (latitudinal slice) or latitude by the altitude (longitudinal slice). The four scenarios are: 1) latitudinal slice at equator; 2) latitudinal slice at 30° S, in the southern crest of the equatorial ionization anomaly (EIA); 3) longitudinal slice at the America Sector (60° W), around 20:00 local time (LT); and 4) longitudinal slice at the Pacific Ocean (160° W), around 13:20 LT. Top panels show the electron density distributions used as reference. Bottom panels show the electron density distributions used as the ionospheric background. The background shows considerable differences in comparison to the distributions assumed as a reference, especially in the daytime and

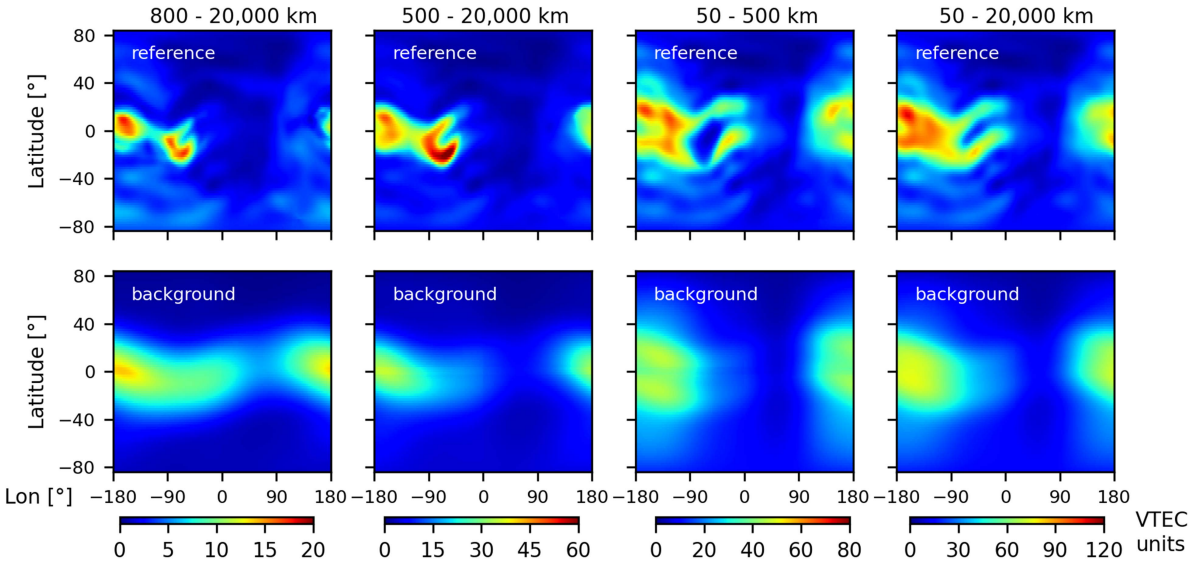

Fig. 3. Background VTEC maps are shown in the bottom row. The values assumed as reference are given in the top row. The simulated TEC measurements are derived by the reference dataset. Four case scenarios are presented: assuming POD observations of LEO satellite at 800 km (800–20 000 km) and 500 km (500–20 000 km); from the ground to the LEO satellites at 500 km (50–500 km); and from the ground to the GNSS altitude (50–20 000 km).

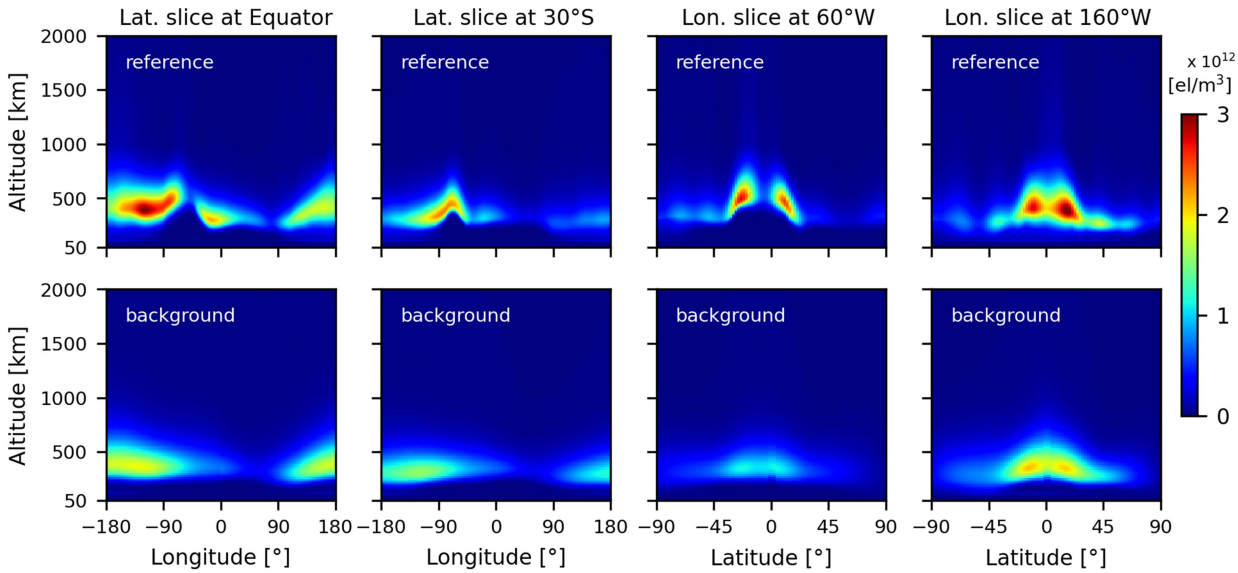

Fig. 4. Background electron density distributions are shown in the bottom row. The values assumed as reference are provided in the top row. Four case scenarios are presented: latitude slices at the equator, latitude slices at 30° S, longitudinal slices at 60° W (referred to 20:00 LT), and longitudinal slices at 160° W (referred to 13:20 LT).

low-latitudes. The main interest of the analysis in the next sections is to show how the LEO satellites can be used to improve the background distributions to obtain distributions like the ones assumed as reference.

B. Simulated TEC Measurements

After having the ionosphere and plasmasphere simulated, the next step is to simulate the ionospheric measurements. In principle, the primary source of ionospheric data provided by LEO-PNT systems is the ionospheric delay, which is inversely proportional to the signal frequency. LEO-PNT systems operating at higher frequencies are less susceptible to ionospheric effects. However, extracting TEC measurements becomes challenging as the ionospheric delay can be obscured by measurement noise. For instance, the K-band is nearly transparent to the ionosphere, making it extremely difficult to extract TEC data. Only with highly accurate measurements is it possible to obtain TEC data in the K-band. A successful example is the GRACE mission, which achieved ranging observations with a precision of approximately 1 μm per second.

While the GRACE mission successfully retrieved TEC measurements in the K-band, for LEO-PNT systems, it is more likely to occur in the L and S bands. However, in our simulations, we

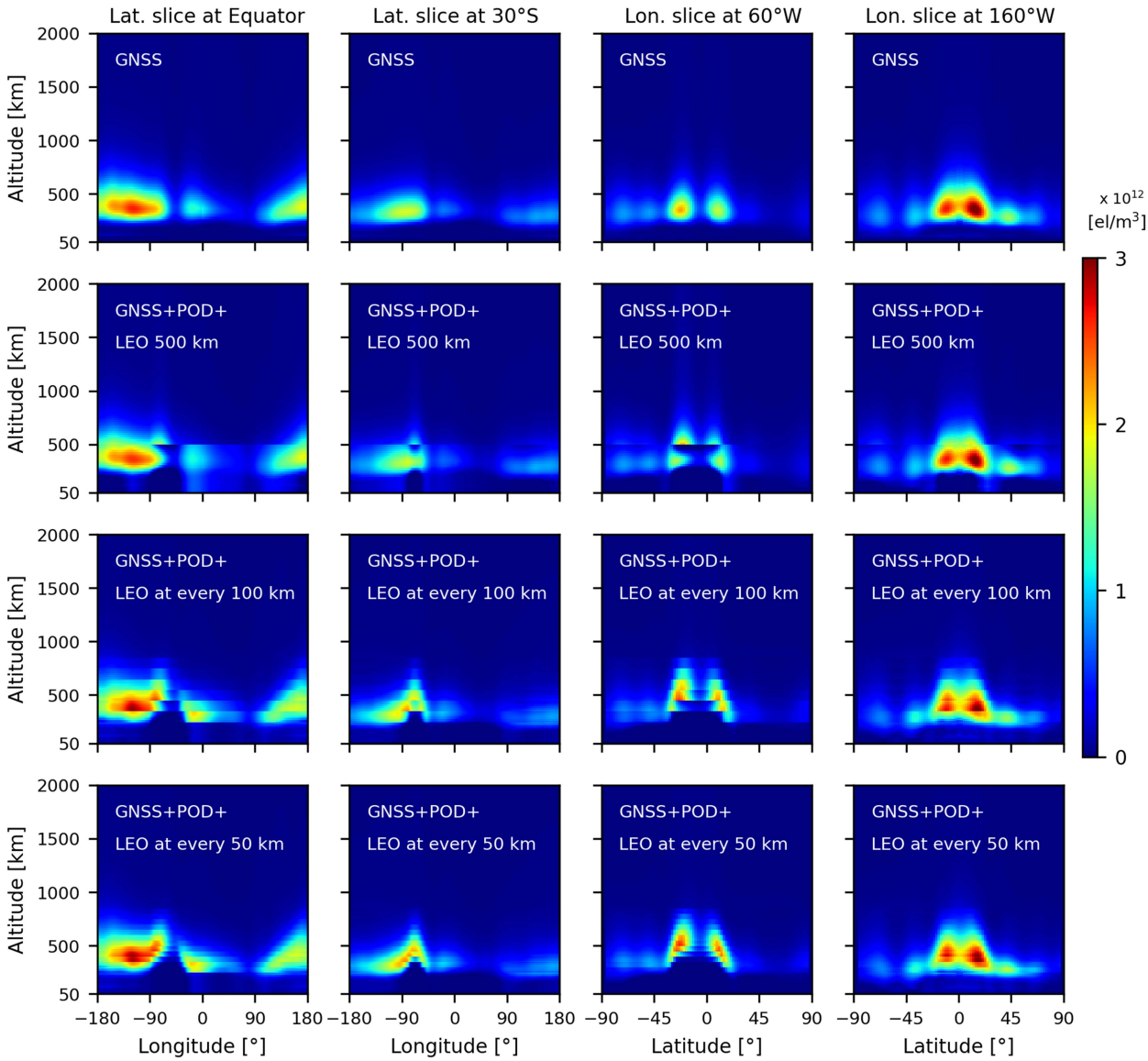

Fig. 5. Electron density profiles estimated with ART by the four geometries described in Table I.

do not impose any specific frequency constraint on the system. The key requirement is that the system is sensitive enough to distinguish between the ionospheric delay and the measurement noise. In addition, no differential code biases (DCBs), ambiguity bias, nor measurements noises are included in the measurements. Our analysis primarily focuses on comprehending the geometric enhancements that LEO satellites can offer to ionospheric tomography. In this regard, the TEC measurements are directly obtained by solving (2) with the electron density values derived from the reference dataset and the integration performed considering the signal as a straight line from the receiver to the transmitter locations.

The satellite transmitters are defined at GNSS and LEO altitudes. To simulate the GNSS satellites, precise GPS, GLONASS, Galileo, and Beidou orbits are obtained from the final IGS products (sp3 files). A total of 113 GNSS satellites are used in further analysis. To simulate the LEO satellite locations, an in-house simulator, named LEO-S9 (LEO simulator with nine modules), is used. The LEO-S9 tool is flexible to create several scenarios of the LEO-PNT space segment, including the LEO orbit dynamics and the satellite payloads. An optimum solution is simulated with a LEO constellation layer of 441 satellites distributed over three orbit inclination planes: 85°, covering mainly the polar region; 55°, covering mostly the mid-latitudes; and 25°, covering the low-latitudes. Several orbit altitudes are simulated to analyze the benefits of using distinct LEO satellites layers. In total, 13 layers of LEO constellations are created in the simulations, ranging from 250 to 850 km, with a step size of 50 km.

As for the receivers, we consider them located on the ground and onboard LEO satellites, so that the LEO satellites act in both ways, i.e., they are both transmitters and receivers. As the main goal is to explore the gains that LEO satellites can bring to a data inversion considering several geometries, no real scenario

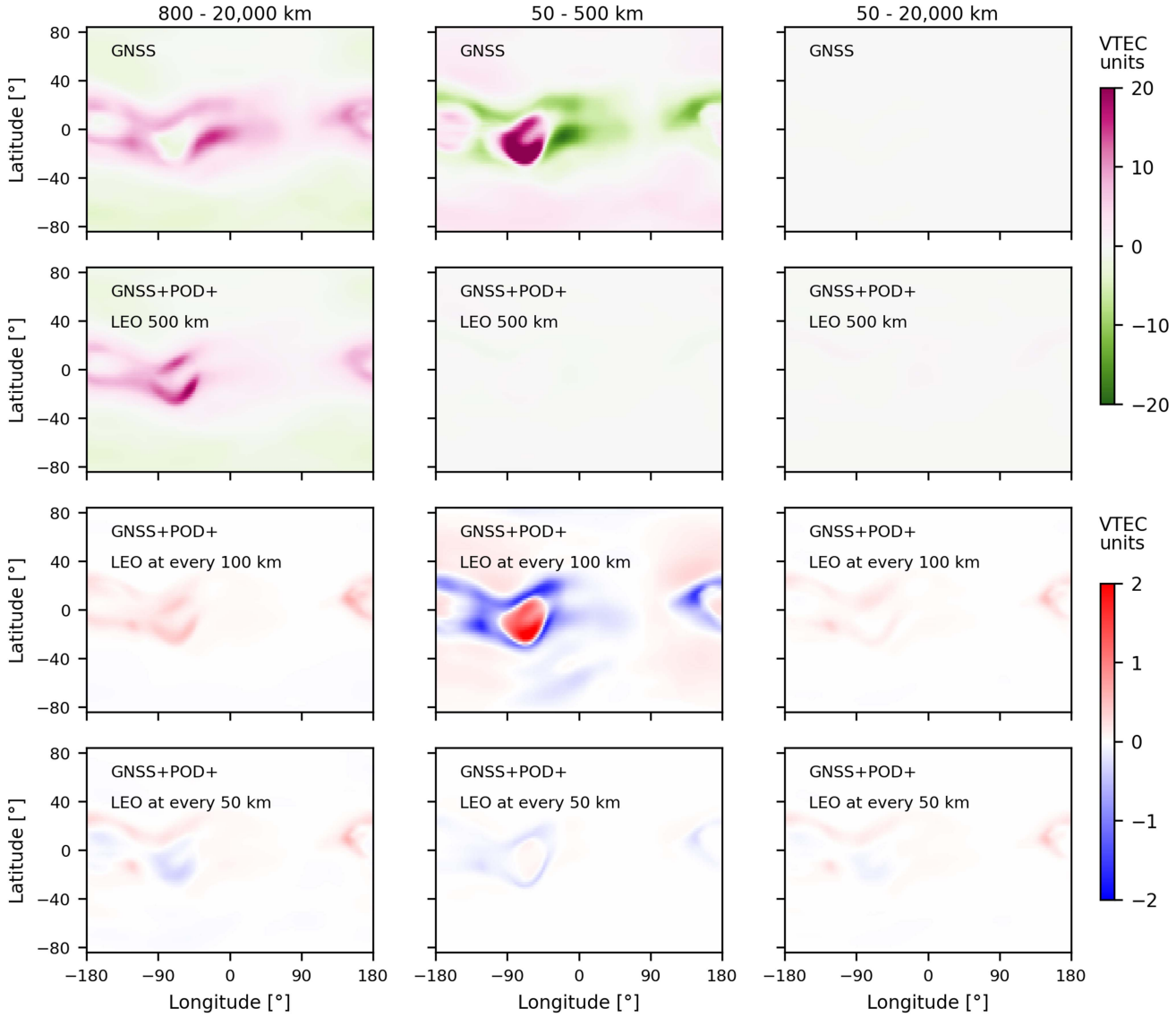

Fig. 6. VTEC error maps of the ART algorithm applied by the four geometries described in Table I.

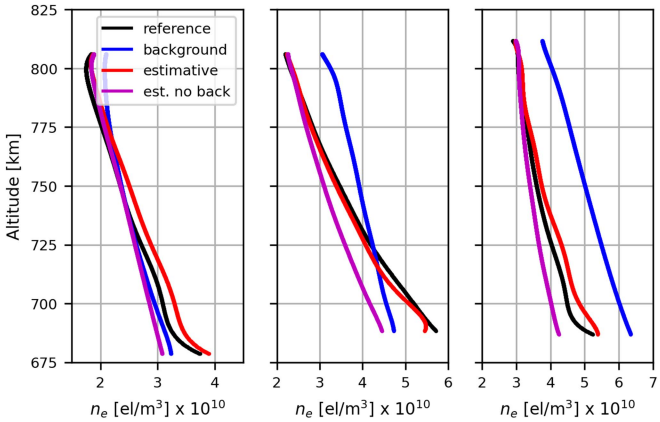

Fig. 7. Examples of electron density ionospheric profiles obtained with the data inversion technique and ISL TEC measurements. The reference and background electron densities are shown for comparison.

of a GNSS network is analyzed. We just assume the ground receivers to be densely distributed. The ground receivers are virtually located every 2° in latitude and longitude, allowing the TEC measurements to cover all voxels of the system. In addition, onboard LEO receivers are simulated to receive data transmitted by other LEO satellites, here referred to as the ISL measurements. This set of measurements opens several opportunities to improve the 3-D ionospheric imaging.

IV. Results

A. TEC Data Inversion by GNSS, LEO POD, and LEO-PNT Measurements

This section analyzes the accuracy of the TEC data inversion technique, ART, when applied to data from ground-based and POD receivers. The visual and numerical analysis is carried out for a total of four configurations combining dedicated LEO-PNT

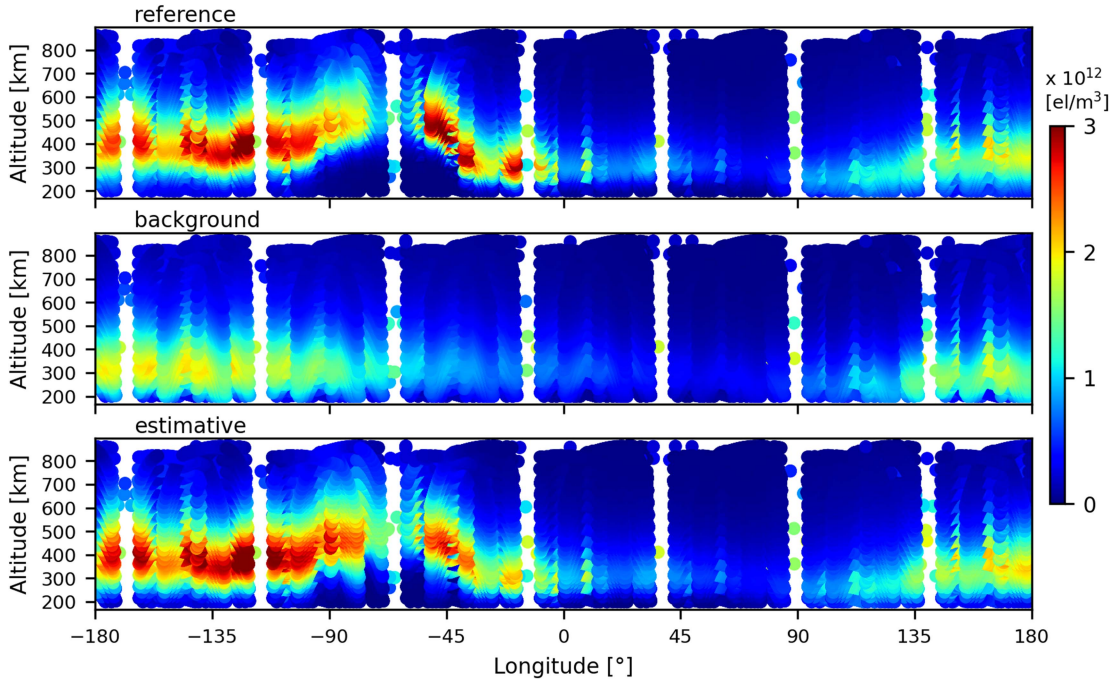

Fig. 8. Electron density estimate by the ISL data inversion (lower panel). Top and middle panels show the reference and background values, respectively.

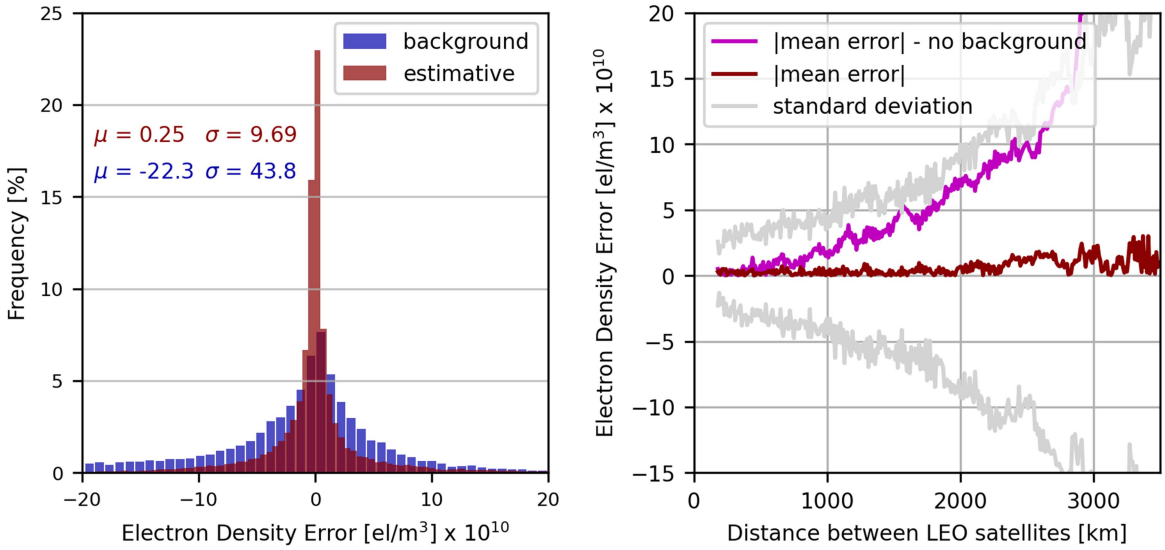

Fig. 9. Electron density distribution of errors obtained with the ISL measurements. The left panel shows the histogram of errors with the background and the developed method. The right panel shows the error variation within the distance between the LEO satellites.

and GNSS systems. Table I shows a brief description of the scenarios. The first one refers to the classical GNSS geometry. The second scenario is defined to represent realistic LEO-PNT systems, where the satellites are defined in one specific orbital altitude. Finally, the third and fourth scenarios represent mega constellations consisting of thousands of LEO satellites distributed across various orbital altitudes.

Fig. 5 shows the main results of electron density distributions obtained with the data inversion algorithm. The panels show distributions similar to those in Fig. 4 for easy comparison. A complete coverage of ground stations is assumed, i.e., the simulated receivers cover all voxels in the system. When using satellites placed at around 20 000 km (GNSS), we can verify that the TEC data inversion mainly updates the background at the peak height. This is expected because the use of only GNSS satellites, makes the system ill-conditioned, updating the background specially at the regions of maximum entropy, i.e., at the regions with the highest electron density. As for the geometry in which we use ground GNSS receiver stations, POD receivers at 800 km, and ground receivers tracking dedicated LEO-PNT systems placed at 500 km, the ionospheric images are mainly updated below the LEO orbit height. Indeed, a sharp transition

TABLE I
GEOMETRY SCENARIOS UTILIZED TO ANALYZE THE TEC DATA INVERSION METHOD

Scenario	Description
GNSS	The TEC data inversion is applied considering the typical GNSS geometry, i.e., the receivers are in the ground and the satellite constellations are composed by GPS, GLONASS, Galileo, and Beidou.
LEO 500 km	The TEC data inversion is applied considering the geometry obtained by three types of observation. Ground-based GNSS measurements, POD observations with LEO satellites at 800 km, and GNSS-like observations transmitted by LEO satellites placed at 500 km and received on the ground.
LEO at every 100 km	In addition to ground-based GNSS measurements and POD observations with LEO satellites at 800 km, the TEC data inversion is applied assuming several LEO satellites transmitting GNSS-like signals to users on the ground. The LEO satellites are placed at every 100-km orbit heights, ranging from 250−850 km. A total of seven LEO layers are formed.
LEO at every 50 km	In addition to ground-based GNSS measurements and POD observations with LEO satellites at 800 km, the TEC data inversion is applied assuming several LEO satellites transmitting GNSS-like signals to users on the ground. The LEO satellites are placed at every 50-km orbit heights, ranging from 250−850 km. A total of 13 LEO layers are formed.

TABLE II
ACCURACY OF THE RETRIEVED TEC, FOF2, AND HMF2 VALUES

Parameter	Background	GNSS	LEO 500 km	LEO 100 km	LEO 50 km
hmF2 [km]	-8.05 ± 34.81	-8.05 ± 34.81	-5.18 ± 28.65	-0.04 ± 25.82	-1.74 ± 18.04
foF2 [MHz]	-0.83 ± 1.54	-0.71 ± 0.83	-0.78 ± 0.97	-0.25 ± 0.32	-0.1 ± 0.18
VTEC [TECU]	-0.97 ± 6.65	-0.06 ± 4.41	-0.03 ± 0.35	-0.04 ± 0.3	-0.01 ± 0.06

The accuracy is represented by the mean ± the standard deviation of the error (model-reference). The VTEC values are computed from 50–500 Km.

exists at 500 km and the algorithm fails to understand the overall morphology of the ionosphere. The TEC data inversion only seems to best represent the vertical distribution of the ionosphere when LEO satellites are placed in distinct layers. For instance, the "LEO 100 km" and "LEO 50 km" geometries shown in Fig. 5 resulted in distributions similar to the reference dataset. We can observe the F-layer reconstruction showing very similar peak heights to the reference dataset and overall good representations of the latitudinal and longitudinal variability. Therefore, in addition to the horizontal distributions, the use of LEO constellations enables to recover the vertical variability of the ionosphere, which has been, so far, an unsolved problem in ionospheric TEC inversion algorithms. In addition, better resolution images are obtained as we use denser satellite constellations, i.e., the TEC data inversion using the "LEO 50 km" geometry outperforms that obtained with the "LEO 100 km" geometry.

Fig. 6 shows the error in three distinct VTEC cases: 1) from 800–20 000 km (left column); 2) from 50 up to 500 km (middle column); and 3) from 50–20 000 km (right column). When using only GNSS satellites, despite that the VTEC error from 50–20 000 km is almost zero, we can observe a VTEC error up to 20 TECU in case the ionosphere is stratified in several layers. This mainly follows from the inability of GNSS-based data inversion to retrieve the vertical distribution of the ionosphere. As we include POD VTEC measurements and LEO satellites at 500 km, the VTEC error reduces at 50–500 km. The error above 800 km is still high since there is no considerable update between 500 and 800 km. In contrast, when using several layers of LEO satellites as dedicated PNT systems, the VTEC error is reduced by one order of magnitude. The maximum error is 2 TECU in the "LEO 100 km" geometry and 1 TECU in the "LEO 50 km" geometry. This improvement is mainly due to the better resolution of the ionospheric vertical distributions.

Table II shows the mean and standard deviation in the analyzed geometries for the errors (data inversion—reference dataset). The parameters used in the evaluation are the hmF2, critical frequency $foF2 = \sqrt{(NmF2/(1.24 * 10^{10}))}$, and VTEC computed from 50–500 km. As expected, the GNSS geometry provides an equal accuracy to the background for the hmF2 estimation. On the other hand, the electron density at the peak (given by foF2) obtained with GNSS agrees much better than the background, with a standard deviation twice lower. In case of the VTEC accuracy (50–500 km), the GNSS measurements improve the background by around 35%. In addition, if LEO satellites are incorporated, the accuracy significantly improves. When using seven layers of LEO satellites at every 100 km, a slight improvement is obtained in the VTEC accuracy. Nevertheless, when using 13 layers of LEO satellites at every 50 km, the VTEC RMSE improves to better than 0.1 TECU. The accuracy of the foF2 parameter improves proportionally to the number of LEO constellation layers. The "LEO 50 km" geometry, for instance, has twice the number of satellites than the "LEO 100 km" geometry and performs twice better as well. In case of the hmF2, the accuracy improves as more LEO satellites are used, but there is a limitation of the estimation to tens of kilometers due to the vertical resolution of the LEO layers being, in the best analyzed scenario, of 50 km.

Previous studies have demonstrated that the performance of hmF2 and foF2 estimation based on TEC data inversion is worse with GNSS due to the almost vertical ray paths [41], [61]. Without having horizontal viewing angles, TEC data inversion fails to reproduce the shape of the ionospheric profiles [23], [62]. However, we use a similar almost vertical geometry in the analysis presented in this section. A cutoff angle of 10° has been included in the POD and LEO-PNT measurements obtained by the virtual receivers. Nevertheless, hmF2 and foF2 has drastically improved in comparison to GNSS. The main improvement in this case was not due to the incorporation of horizontal signals. By placing the satellites in different layers and having only vertical viewing angles, the TEC inversion techniques can distribute the electron density over the ionospheric profiles and better estimate the profile shapes. This is indeed

unique in the field of ionospheric modeling. In medicine, for instance, inversion techniques like tomography [63], [64] are carried out at different viewing angles (horizontal, tilted, and vertical). There is no opportunity to incorporate sensors inside the object of interest, as in the present study.

B. TEC Data Inversion by ISL Measurements

This section analyzes the accuracy of the TEC data inversion technique developed to retrieve the electron density values from ISL data between LEO satellites. Fig. 7 shows an example of the electron density profiles estimated with the developed technique based on (6). For comparison, ionospheric profiles are also shown for the reference values, background, and retrieved with (5), called "est. no back." This example considers two satellites placed at 800-km orbital heights, with an initial distance lower than 200 km in the first ISL observation (around 800-km height) and final distance larger than 2000 km (around 675-km height). We verify that the electron density values obtained with the developed method are much closer to the reference values at higher altitudes, where the LEO satellites are closer. At lower altitudes, a slightly worse performance is observed with the proposed method (red lines in Fig. 7), and an evident lower accuracy is obtained when not using the background (magenta lines). Despite the background (blue line) is relatively far from the reference electron density profiles, the technique is still able to reproduce the horizontal gradients of the ionosphere and help the estimator. This example highlights the benefits of using (6) rather than (5).

To verify the capabilities of the developed technique for obtaining 3-D images of the ionosphere, Fig. 8 shows the latitudinal slice of the equatorial ionosphere when using the best behaving geometry of the previous section (LEO at every 50 km). The equatorial region is selected for this analysis since it is a challenging region to represent by any ionospheric imaging system. A dense constellation is used to obtain the reconstructions, with around 5700 LEO satellites distributed over three inclination planes (85°, 55°, 25°). A high number of satellites is required because few pairs of satellites do attend the minimum requirement of the developed technique. There are just a few satellites that are close enough ($<$200 km) to each other in the initial electron density retrievals. Even with this highly dense constellation, gaps in the electron density are still caused by lack of data at specific longitudes.

Overall, the developed technique can recover most of the electron density distributions derived from the reference dataset. We can see similar magnitude and morphology of the electron density distributions, showing that the low accuracy of the background was not a major issue in the reconstruction. The estimations presented lower performance only at the prereversal period located at around -90° to -45° in longitude. The reference dataset has shown the peak height to be around 500 km in the most active locations, while the background presented a peak height of around 300 km. The developed method produced an intermediate peak height value of around 400 km during the prereversal period. Hence, the developed technique is less accurate at the locations where the background completely fails to represent the peak height and the consequent horizontal gradients of the region. If the observation dataset is dense enough to update the background at every location, a few iterations over the estimation process will likely solve the problem.

The general accuracy of the developed technique assuming a highly dense LEO constellation is presented in Fig. 9. The left panel shows no bias, presenting a mean error of $0.25*10^{10}$ el/m^3 while the background has shown a negative bias of $-22.3*10^{10}$ el/m^3. The total RMSE obtained is $9.69*10^{10}$ el/m^3 and $43.8*10^{10}$ el/m^3 for the developed technique and background, respectively, showing an improvement of around 80% over the background. Fig. 9 (right panel) also shows the electric density error in terms of the distance between the LEO satellites. The absolute mean error tends to remain with no bias even when the LEO satellites are far apart. However, the standard deviation of the error is severely affected. This means that the misrepresentation of the background makes the error dispersive but centered at zero. For comparison, the magenta line shows the same error obtained when applying (5) to estimate the electron density, with no background included. The mean error deviates from the actual ionosphere with an increasing bias as the distance between the LEO satellites increase. As the ionospheric horizontal gradients are not corrected in (5), the error proportionally increases with the intersatellite distances.

V. Conclusion

Simulated results were produced to investigate the benefits that mega LEO-PNT constellations can provide to 3-D ionospheric imaging. We simulated TEC measurements using ground-based receivers, GNSS satellites, and LEO satellites acting in both ways, as transmitters and receivers. We first analyzed the accuracy of 3-D imaging methods when using TEC observations obtained from ground GNSS receivers, GNSS receivers onboard LEO satellites primarily made for POD, and LEO-PNT ground receivers. Then, we developed a technique to derive electron density values based on ISL range measurements. The analysis was carried out considering the current GNSS geometry, a realistic LEO-PNT dedicated constellation, and a mega constellation composed by thousands of LEO satellites. The main conclusions are the following.

1) Ionospheric tomography techniques based on LEO satellites can provide highly accurate electron density reconstructions. This means that the ill-condition geometry typically observed in GNSS-based ionospheric tomography can be overcome by using data from LEO satellites. However, to improve the current climatological models using TEC data ingestion, several LEO satellites are required. In our experiments, a reconstruction that allows imaging the main variations of the ionosphere would require around 5700 LEO satellites deployed at every 50 km, ranging from 250–850 km. A more realistic scenario with only an orbit plane at 500 km and 441 satellites was also simulated, but it was not enough to solve the 3-D imaging problem. To recover the main variations of the ionosphere, the ionospheric 3-D imaging requires much more than a single LEO layer dedicated for PNT.

2) Our investigation has also shown that TEC data inversion algorithms can provide accurate representation of the ionosphere without using horizontal viewing angles. This is typically impossible in other fields using tomography techniques (e.g., medicine) because a transmitter, usually, cannot be deployed inside the object of interest. When there are several LEO satellites inside the ionosphere as a transmitter, the tomographic algorithm can distinguish the different ionospheric layers and recover the electron density profiles, mainly at the peak height and topside ionosphere, due to the geometric gains in the system.
3) The intersatellite links providing ranging measurements can bring benefits to the 3-D ionospheric imaging. We have proposed a method which exploits the ISL geometry between LEO satellites and computes accurate electron density values. The developed method is inspired by the electron density retrievals from the GRACE satellite data; however, our investigation has shown that a background may be required to correct the nonsymmetric assumption of the ionosphere and further improve the ISL estimations. No evident bias was obtained in the estimation, but a lower accuracy was observed in regions where the background completely fails to represent the peak height.

As the simulations were carried out with an optimum scenario of ground-based GNSS receivers and a fully controlled ionospheric simulation, the results presented in this work serve of gains from the system geometry. There are still additional issues to analyze, such as the impact of the measurement noises, data gaps, background accuracy, and distinct ionospheric conditions due to seasons, solar cycle, and storm events. A feasible number of LEO satellites is also a relevant point for the future analysis, considering the mission cost, end user applications, and optimization strategy. Our current work is also constrained by the inability to utilize LEO satellites below 250 km, which may affect the 3-D imaging in case of lower hmF2 values.

An important aspect to consider for future analysis is the integration of physics-based models into our simulations. The incorporation of such models is essential as they enable the simulation of small-scale structures within the ionosphere, facilitating the analysis of the ionosphere mapping process under the influence of geomagnetic storms. We have also not addressed the TEC calibration issue yet. Indeed, the best technique to calibrate the TEC measurements will depend on the overall LEO-PNT system constellation and instruments, as the TEC calibration accuracy depends on several factors, such as the system frequency, orbital height, number of ground stations, and whether any external data sources can be used as reference. If accurate TEC measurements are obtained, this study has shown that LEO satellites can bring relevant gains to the 3-D ionospheric imaging. The analysis can also serve as a guideline to promote new satellite missions specifically designed to improve ionospheric modeling.

REFERENCES

[1] I. del Portillo, B. G. Cameron, and E. F. Crawley, "A technical comparison of three low Earth orbit satellite constellation systems to provide global broadband," *Acta Astronautica*, vol. 159, pp. 123–135, 2019.

[2] I. Leyva-Mayorga et al., "LEO small-satellite constellations for 5G and beyond-5G communications," *IEEE Access*, vol. 8, pp. 184955–184964, 2020.

[3] M. J. M. Kiki and I. Iddi, "Improved LORA modulation output in LEO satellite Internet of Things," *J. Elect. Eng. Technol.*, vol. 17, pp. 1379–1387, 2022.

[4] L. Wang et al., "Initial assessment of the LEO based navigation signal augmentation system from Luojia-A1 satellite," *Sensors*, vol. 18, no. 11, 2018, Art. no. 3919.

[5] T. G. Reid, A. M. Neish, T. Walter, and P. K. Enge, "Broadband LEO constellations for navigation," *Navigation*, vol. 65, no. 2, pp. 205–220, 2018.

[6] B. Li, H. Ge, M. Ge, L. Nie, Y. Shen, and H. Schuh, "LEO enhanced global navigation satellite system (LeGNSS) for real-time precise positioning services," *Adv. Space Res.*, vol. 63, no. 1, pp. 73–93, 2019.

[7] T. G. Reid et al., "Satellite navigation for the age of autonomy," in *Proc. IEEE/ION Position, Location, Navigation Symp.*, 2020, pp. 342–352.

[8] R. M. Ferre et al., "Is LEO-based positioning with mega-constellations the answer for future equal access localization?," *IEEE Commun. Mag.*, vol. 60, no. 6, pp. 40–46, Jun. 2022.

[9] C. Shi, Y. Zhang, and Z. Li, "Revisiting Doppler positioning performance with LEO satellites," *GPS Solutions*, vol. 27, 2023, Art. no. 126.

[10] F. S. Prol et al., "Position, navigation, and timing (PNT) through low Earth orbit (LEO) satellites: A survey on current status, challenges, and opportunities," *IEEE Access*, vol. 10, pp. 83971–84002, 2022.

[11] H. Ge et al., "LEO enhanced global navigation satellite system (LeGNSS): Progress, opportunities, and challenges," *Geo-Spatial Inf. Sci.*, vol. 25, no. 1, pp. 1–13, 2022.

[12] J. Rainbow, "Lockheed invests in Xona's GPS-alternative constellation," Accessed on: May 15, 2023. [Online]. Available: https://spacenews.com/lockheed-invests-in-xonas-gps-alternative-constellation/

[13] R. Knight, "ESA outlines plans for demo of LEO PNT satellites as part of FutureNAV, gives other updates," Accessed on: May 15, 2023. [Online]. Available: https://insidegnss.com/

[14] L. Chen et al., "Signal acquisition of Luojia-A1 low Earth orbit navigation augmentation system with software defined receiver," *Geo-Spatial Inf. Sci.*, vol. 25, no. 1, pp. 47–62, 2022.

[15] "Project indoor navigation from CubeSat technology (INCUBATE)," Accessed on: May 15, 2023. [Online]. Available: https://www.incubateproject.org/

[16] P. A. Iannucci and T. E. Humphreys, "Fused low-Earth-orbit GNSS," *IEEE Trans. Aerosp. Electron. Syst.*, to be published, doi: 10.1109/TAES.2022.3180000.

[17] T. G. Reid, A. M. Neish, T. F. Walter, and P. K. Enge, "Leveraging commercial broadband LEO constellations for navigating," in *Proc. 29th Int. Tech. Meeting Satell. Division Inst. Navigation*, 2016, pp. 2300–2314.

[18] J. Khalife, M. Neinavaie, and Z. M. Kassas, "The first carrier phase tracking and positioning results with Starlink LEO satellite signals," *IEEE Trans. Aerosp. Electron. Syst.*, vol. 58, no. 2, pp. 1487–1491, Apr. 2022.

[19] X. Ren, J. Zhang, J. Chen, and X. Zhang, "Global ionospheric modeling using multi-GNSS and upcoming LEO constellations: Two methods and comparison," *IEEE Trans. Geosci. Remote Sens.*, vol. 60, 2022, Art. no. 5800215.

[20] A. L. Christovam, F. Prol, M. Hernández-Pajares, and P. O. Camargo, "Plasma bubble imaging by single-frequency GNSS measurements," *GPS Solutions*, vol. 27, 2023, Art. no. 124.

[21] M. Hernández-Pajares et al., "The IGS VTEC maps: A reliable source of ionospheric information since 1998," *J. Geodesy*, vol. 83, pp. 263–275, 2009.

[22] G. S. Bust and C. N. Mitchell, "History, current state, and future directions of ionospheric imaging," *Rev. Geophys.*, vol. 46, 2008, Art. no. RG1003, doi: 10.1029/2006RG000212.

[23] F. S. Prol, P. O. Camargo, and M. T. A. H. Muella, "Numerical simulations to assess ART and MART performance for ionospheric tomography of chapman profiles," *Academia Brasileira de Ciências*, vol. 89, no. 3, pp. 1531–1542, 2017.

[24] D. Wen, D. Mei, and Y. Du, "Adaptive smoothness constraint ionospheric tomography algorithm," *Sensors*, vol. 20, no. 8, 2020, Art. no. 2404.

[25] F. S. Prol, T. Kodikara, M. M. Hoque, and C. Borries, "Global-scale ionospheric tomography during the Mar. 17, 2015 geomagnetic storm," *Space Weather*, vol. 19, no. 12, 2021, Art. no. e2021SW002889.

[26] D. Mei, X. Ren, X. Le, H. Liu, and X. Zhang, "Ionospheric tomography: A compressed sensing technique based on dictionary learning," *IEEE Trans. Geosci. Remote Sens.*, vol. 61, 2023, Art. no. 5800410.

[27] J. Norberg, S. Käki, L. Roininen, J. Mielich, and I. I. Virtanen, "Model-free approach for regional ionospheric multi-instrument imaging," *J. Geophys. Res.: Space Phys.*, vol. 128, no. 1, 2023, Art. no. e2022JA030794.
[28] B. Nava, S. M. Radicella, and F. Azpilicueta, "Data ingestion into NeQuick 2," *Radio Sci.*, vol. 46, no. 6, pp. 1–8, 2011.
[29] E. Aa, S.-R. Zhang, P. J. Erickson, W. Wang, A. J. Coster, and W. Rideout, "3-D regional ionosphere imaging and SED reconstruction with a new TEC-based ionospheric data assimilation system (TIDAS)," *Space Weather*, vol. 20, no. 4, 2022, Art. no. e2022SW003055.
[30] G. Bust and T. Immel, "IDA4D: Ionospheric data assimilation for the ICON mission," *Space Sci. Rev.*, vol. 216, 2020, Art. no. 33.
[31] R. Garcia and F. Crespon, "Radio tomography of the ionosphere: Analysis of an underdetermined, ill-posed inverse problem, and regional application," *Radio Sci.*, vol. 43, no. 2, pp. 1–13, 2008.
[32] M. Ananda, H. Bernstein, K. Cunningham, W. Feess, and E. Stroud, "Global positioning system (GPS) autonomous navigation," in *Proc. IEEE Symp. Position Location Navigation. A Decade Excellence Navigation Sci.*, 1990, pp. 497–508.
[33] X. Xie et al., "Precise orbit determination for BDS-3 satellites using satellite-ground and inter-satellite link observations," *GPS Solutions*, vol. 23, 2019, Art. no. 40.
[34] Y. Yang et al., "Inter-satellite link enhanced orbit determination for Beidou-3," *J. Navigation*, vol. 73, no. 1, pp. 115–130, 2020.
[35] A. Schlicht, S. Marz, M. Stetter, U. Hugentobler, and W. Schäfer, "Galileo pod using optical inter-satellite links: A simulation study," *Advances. Space Res.*, vol. 66, no. 7, pp. 1558–1570, 2020.
[36] T. Kur and M. Kalarus, "Simulation of inter-satellite link schemes for use in precise orbit determination and clock estimation," *Adv. Space Res.*, vol. 68, no. 12, pp. 4734–4752, 2021.
[37] X. Li, Z. Jiang, F. Ma, H. Lv, Y. Yuan, and X. Li, "LEO precise orbit determination with inter-satellite links," *Remote Sens.*, vol. 11, no. 18, 2019, Art. no. 2117.
[38] G. Lalgudi Gopalakrishnan and M. Schmidt, "Ionospheric electron density modelling using B-splines and constraint optimization," *Earth Planets Space*, vol. 74, 2022, Art. no. 143.
[39] H. Le, T. Han, Q. Li, L. Liu, Y. Chen, and H. Zhang, "A new global ionospheric electron density model based on grid modeling method," *Space Weather*, vol. 20, no. 6, 2022, Art. no. e2021SW002992.
[40] E. Aa, V. V. Forsythe, S.-R. Zhang, W. Wang, and A. J. Coster, "Next-decade needs for 3-D ionosphere imaging," *Front. Astron. Space Sci.*, vol. 10, 2023, Art. no. 1186513.
[41] J. R. Austen, S. J. Franke, and C. H. Liu, "Ionospheric imaging using computerized tomography," *Radio Sci.*, vol. 23, no. 3, pp. 299–307, 1988.
[42] T. Panicciari, N. D. Smith, C. N. Mitchell, F. Da Dalt, and P. S. J. Spencer, "Using sparse regularization for multi-resolution tomography of the ionosphere," *Nonlinear Processes Geophys.*, vol. 22, no. 5, pp. 613–624, 2015.
[43] D. Wen, S. Liu, and P. Tang, "Tomographic reconstruction of ionospheric electron density based on constrained algebraic reconstruction technique," *GPS Solutions*, vol. 14, pp. 375–380, 2010.
[44] F. S. Prol, M. M. Hoque, and A. A. Ferreira, "Plasmasphere and topside ionosphere reconstruction using METOP satellite data during geomagnetic storms," *J. Space Weather Space Climate*, vol. 11, 2021, Art. no. 5.
[45] F. S. Prol and M. M. Hoque, "A tomographic method for the reconstruction of the plasmasphere based on COSMIC/ FORMOSAT-3 data," *IEEE J. Sel. Topics Appl. Earth Observ. Remote Sens.*, vol. 15, pp. 2197–2208, 2022.
[46] R. Ruan et al., "Orbit determination and time synchronization for BDS-3 satellites with raw inter-satellite link ranging observations," *Satell. Navigation*, vol. 1, 2020, Art. no. 8.
[47] N. Jakowski et al., "GPS radio occultation measurements of the ionosphere from champ: Early results," *Geophys. Res. Lett.*, vol. 29, no. 10, pp. 95-1–95-4, 2002.
[48] M. M. Hoque et al., "A new method of electron density retrieval from MetOp–A's truncated radio occultation measurements," *Remote Sens.*, vol. 15, no. 5, 2023, Art. no. 1424.
[49] M. Shaikh, R. Notarpietro, and B. Nava, "The impact of spherical symmetry assumption on radio occultation data inversion in the ionosphere: An assessment study," *Adv. Space Res.*, vol. 53, no. 4, pp. 599–608, 2014.
[50] G. A. Hajj and L. J. Romans, "Ionospheric electron density profiles obtained with the global positioning system: Results from the GPS/MET experiment," *Radio Sci.*, vol. 33, no. 1, pp. 175–190, 1998.
[51] W. S. Schreiner, S. V. Sokolovskiy, C. Rocken, and D. C. Hunt, "Analysis and validation of GPS/MET radio occultation data in the ionosphere," *Radio Sci.*, vol. 34, no. 4, pp. 949–966, 1999.
[52] P. Guo, M. Wu, T. Xu, H. Jin, and X. Hu, "An Abel inversion method assisted by background model for GPS ionospheric radio occultation data," *J. Atmospheric Sol.-Terrestrial Phys.*, vol. 123, pp. 71–81, 2015.
[53] C. Xiong, J. Park, H. Lühr, C. Stolle, and S. Y. Ma, "Comparing plasma bubble occurrence rates at champ and grace altitudes during high and low solar activity," *Anales Geophysicae*, vol. 28, no. 9, pp. 1647–1658, 2010.
[54] C. Xiong, H. Lühr, S. Ma, and K. Schlegel, "Validation of grace electron densities by incoherent scatter radar data and estimation of plasma scale height in the topside ionosphere," *Adv. Space Res.*, vol. 55, no. 8, pp. 2048–2057, 2015.
[55] M. M. Hoque, N. Jakowski, and F. S. Prol, "A new climatological electron density model for supporting space weather services," *J. Space Weather Space Climate*, vol. 12, 2022, Art. no. 1.
[56] D. Bilitza et al., "International reference ionosphere 2016: From ionospheric climate to real-time weather predictions," *Space Weather*, vol. 15, no. 2, pp. 418–429, 2017.
[57] A. Smirnov et al., "A novel neural network model of Earth's topside ionosphere," *Sci. Rep.*, vol. 13, 2023, Art. no. 1303.
[58] F. S. Prol, A. G. Smirnov, M. M. Hoque, and Y. Y. Shprits, "Combined model of topside ionosphere and plasmasphere derived from radio-occultation and Van Allen Probes data," *Sci. Rep.*, vol. 12, 2022, Art. no. 9732.
[59] C. Xiong et al., "Solar flux influence on the in-situ plasma density at topside ionosphere measured by swarm satellites," *J. Geophys. Res.: Space Phys.*, vol. 127, no. 5, 2022, Art. no. e2022JA030275.
[60] G. O. Jerez et al., "Two-way assessment of ionospheric maps performance over the Brazilian region: Global versus regional products," *Space Weather*, vol. 21, no. 2, 2023, Art. no. e2022SW003252.
[61] C. N. Mitchell, L. Kersley, J. A. T. Heaton, and S. E. Pryse, "Determination of the vertical electron-density profile in ionospheric tomography: Experimental results," *Anales Geophysicae*, vol. 15, no. 6, pp. 747–752, 1997.
[62] J. Bruno, C. N. Mitchell, K. H. Bolmgren, and B. A. Witvliet, "A realistic simulation framework to evaluate ionospheric tomography," *Adv. Space Res.*, vol. 65, no. 3, pp. 891–901, 2020.
[63] H. Lauridsen et al., "Inside out: Modern imaging techniques to reveal animal anatomy," *PLoS One*, vol. 6, no. 3, 2011, Art. no. e17879.
[64] J. Wang, J. Liang, J. Cheng, Y. Guo, and L. Zeng, "Deep learning based image reconstruction algorithm for limited-angle translational computed tomography," *PLoS One*, vol. 15, no. 1, 2020, Art. no. e0226963.

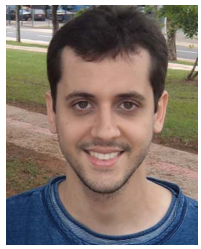

Fabricio S. Prol received the Ph.D. degree in cartographic sciences from the São Paulo State University, São Paulo, Brazil, with focus in geodetic remote sensing and geodetic positioning, in 2019.

He has been working with the Finnish Geospatial Research Institute, Helsinki, Finland, since 2021. His research interests include ionospheric modeling, GNSS positioning, LEO-PNT navigation, and data assimilation.

Artem Smirnov is a doctoral candidate in Computational Physics working at the GFZ German Research Centre for Geosciences in Potsdam. He received a bachelor's degree in geophysics from the Lomonosov Moscow State University, in 2017, and a joint master's degree in geophysics from LMU and TUM in 2019.

His research interests are primarily focused on data analysis and empirical modeling of plasma populations in the ionosphere and inner magnetosphere of the Earth using machine learning.

Sanna Kaasalainen received the Ph.D. degree in astronomy from the University of Helsinki, Helsinki, Finland, in 2003.

She is currently a Professor and Head of the Department of Navigation and Positioning, FGI of the National Land Survey, Helsinki, Finland. Her research interests include resilient positioning, navigation, and timing, situational awareness, and optical sensors. She also has research experience in LIDAR remote sensing, sensor development, and astronomy.

Mohammad Mainul Hoque received the bachelor's degree in electrical and electronics engineering and the Ph.D. degree in engineering science from the University of Siegen, Germany, in 2000 and 2009, respectively.

He has been working on ionosphere and plasmasphere modeling, propagation effects modeling including higher order terms with the German Aerospace Center (DLR), Cologne, Germany, since 2004. Since 2019, he has been working as the Head of the Department for Space Weather Observations, Institute for Solar-Terrestrial Physics, DLR. He was/is involved and has contributed in many national, international as well as ESA and EU projects related to ionosphere modeling and propagation delay corrections. He has authored/coauthored of three patents and over 80 scientific papers in referred journals.

Mohammad Zahidul H. Bhuiyan received the Ph.D. degree in communications engineering from the Tampere University of Technology (TUT), Tampere, Finland, in 2007.

He is a Research Professor with the Department of Navigation and Positioning, Finnish Geospatial Research Institute, Helsinki, Finland. He is actively involved in teaching GNSS-related courses with Finnish universities and other training schools. He has been also working as a Technical Expert with the EU Agency for the Space Program in H2020 project reviewing and proposal evaluation. His research interests include multi-GNSS receiver development, PNT robustness and resilience, and seamless positioning, etc.

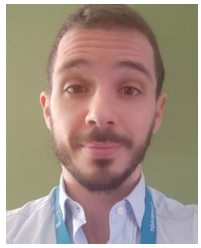

Francesco Menzione received the B.E., M.E., and Ph.D. degrees in aerospace engineering and satellite navigation from the University of Naples Federico II, Naples, Italy, in 2009, 2012, and 2017, respectively.

After almost eight years working in the Aerospace sector, he joined the European Commission Joint Research Centre as Technical and Scientific Officer for the Galileo Sector. He is currently contributing to different projects in the context of EU next generation space programme. His research interests include GNSS navigation, precise orbit determination, space service volume, and LEO PNT systems.